ACS SyntheticBiology

Research Article

pubs.acs.org/synthbio

Biophysical, Mutational, and Functional Investigation of the Chromophore-Binding Pocket of Light-Oxygen-Voltage Photoreceptors

Ralph P. Diensthuber,[†,§] Christopher Engelhard,[‡,§] Nora Lemke,[†] Tobias Gleichmann,[†,∥] Robert Ohlendorf,[†] Robert Bittl,*[,‡] and Andreas Möglich*[,†]

[†]Humboldt-Universität zu Berlin, Institut für Biologie, Biophysikalische Chemie, 10115 Berlin, Germany

[‡]Freie Universität Berlin, Fachbereich Physik, Institut für Experimentalphysik, 14195 Berlin, Germany

ABSTRACT: As light-regulated actuators, sensory photoreceptors underpin optogenetics and numerous applications in synthetic biology. Protein engineering has been applied to fine-tune the properties of photoreceptors and to generate novel actuators. For the blue-light-sensitive light-oxygen-voltage (LOV) photoreceptors, mutations near the flavin chromophore modulate response kinetics and the effective light responsiveness. To probe for potential, inadvertent effects on receptor activity, we introduced these mutations into the engineered LOV photoreceptor YF1 and determined their impact on light regulation. While several mutations severely impaired the dynamic range of the receptor (e.g., I39V, R63K, and N94A), residue substitutions in a second group were benign with little effect on regulation (e.g., V28T, N37C, and L82I). Electron paramagnetic resonance and absorption spectroscopy identified correlated effects for certain of the latter mutations on chromophore environment and response kinetics in YF1 and the LOV2 domain from *Avena sativa* phototropin 1. Carefully chosen mutations provide a powerful means to adjust the light-response function of photoreceptors as demanded for diverse applications.

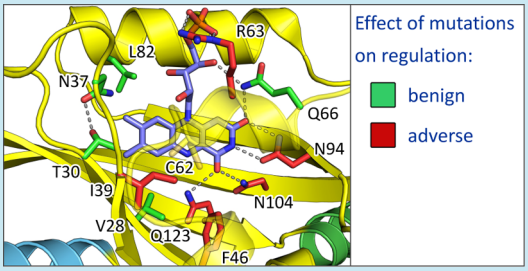

KEYWORDS: *absorption spectroscopy, electron paramagnetic resonance, light-oxygen-voltage, optogenetics, photocycle, photoreceptor, signal transduction*

The perception of environmental light is pivotal for many organisms, as light provides precise spatial and temporal cues that allow initiation of adequate behavioral and physiological responses.[1] The molecular identification of sensory photoreceptor proteins as the agents mediating light sensation paved the way toward both their detailed biophysical characterization and their recent application in synthetic biology. At the functional level, sensory photoreceptors comprise photosensor and effector modules, where the photosensor binds an organic chromophore via which it absorbs light, and the effector harbors biological activity (e.g., DNA-binding or enzymatic).[2] The photosensor unit interacts with the effector unit in a light-dependent manner and thus modulates its biological activity; put another way, all photoreceptors are light-switchable proteins. It is for this attractive property that sensory photoreceptors have recently seen widespread use in cell biology, neuroscience, biotechnology, and synthetic biology. Crucially, photoreceptors commonly employ chromophores that are widely abundant metabolites (e.g., flavin nucleotides or retinal) and autonomously incorporate them. Thus, no exogenous chromophores or other factors are required, and photoreceptors can readily be introduced to diverse target cells and organisms as DNA templates where they are functionally expressed *in situ*. Target cells and organisms are thereby rendered light-responsive and can be manipulated by light in spatiotemporally precise, reversible, and noninvasive fashion. Initially, this approach, dubbed optogenetics,[3] solely relied on naturally occurring rhodopsin photoreceptors that act as light-gated ion channels[4] or light-driven ion pumps.[5] Motivated by the immediate and strong impact of optogenetics, researchers have sought to expand the repertoire of light-regulated proteins beyond the set of natural photoreceptors.[2] Novel photoreceptors with customized light-dependent function have been engineered via recombination of photosensor modules that respond to the desired light quality with effector modules that harbor the desired biological activity. While the specifics widely differ, all approaches exploit that sensor and effector functionalities often reside in distinct regions or domains of the intact photoreceptor and that they hence become physically separable.

Particularly many engineering approaches and subsequent optogenetic applications (e.g., to control cell motility[6] or gene expression by light)[7] depend on blue-light receptors of the light-oxygen-voltage[8,9] (LOV) class, which bind flavin-nucleotide chromophores. Light absorption in the blue spectral region by the dark-adapted state D_{447} initiates the photocycle, a series

Special Issue: Synthetic Photobiology

Received: December 13, 2013
Published: February 20, 2014

   dx.doi.org/10.1021/sb400205x | *ACS Synth. Biol.* 2014, 3, 811–819

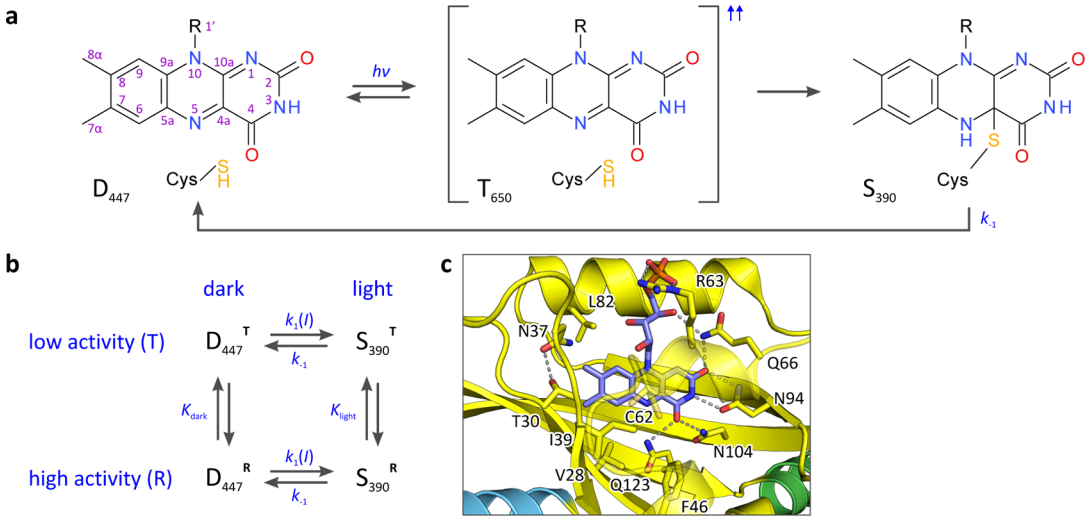

Figure 1. (a) Simplified photocycle of LOV photoreceptors. Upon blue-light absorption by the dark-adapted state D_{447}, the flavin chromophore undergoes efficient intersystem crossing to form the transiently populated triplet state T_{650}, indicated by the two upward arrows (↑↑). Formation of a thioether bond to a conserved cysteine residue within the LOV photosensor yields the signaling state S_{390} which thermally reverts to the dark-adapted ground state with rate constant k_{-1}. Atom numbers of the flavin-nucleotide chromophore are indicated. (b) Thermodynamic model for photoreceptor signaling. The LOV photoreceptor is in dynamic equilibrium between two states of low and high biological activity, denoted T and R, respectively. Light absorption changes the equilibrium between T and R from K_{dark} in the dark to K_{light} and thereby modulates the overall biological activity. (c) Location of residues in YF1 (PDB entry 4GCZ[32]) that were reported to influence the dark recovery kinetics when mutated (cf. Table 1). Dashed gray lines denote hydrogen bonds or salt bridges; the active-site cysteine 62 displays two alternate conformations.

of photochemical reactions[10,11] (Figure 1a). Via the transiently populated triplet state T_{650}, the signaling state S_{390} is assumed in which atom Sγ of a conserved cysteine residue in the LOV photosensor forms a covalent bond to atom C4a of the isoalloxazine ring of the flavin chromophore.[12] The signaling state S_{390} is relatively long-lived and thermally reverts to the ground state D_{447} over tens to ten thousands of seconds depending on LOV domain. In the case of the arguably best studied representative, the LOV2 domain from *Avena sativa* phototropin 1 (*As*LOV2), light absorption promotes reversible unfolding of a C-terminal α helix, denoted Jα, leading to regulation of a downstream effector module.[13] However, nuclear magnetic resonance spectroscopy revealed that the Jα helix exists as an intrinsic equilibrium mixture between folded and unfolded states both in the absence and in the presence of light,[14,15] similar to observations for other signal receptors.[16] Based on the activity of the associated effector, we denote these states as T (tense, lower activity) and R (relaxed, higher activity)[17,18] (Figure 1b); the net activity of the receptor is determined by the balance between T and R. Adoption of the signaling state upon light absorption merely shifts the dynamic equilibrium between T and R from K_{dark} to K_{light} but does not alter the states *per se*. Under constant illumination at a given irradiance *I*, a photoinduced equilibrium between S_{390} and D_{447} is attained, given by the ratio of the rate constants for the light-driven forward reaction, $k_1(I)$, and the thermal back reaction, k_{-1} (Figure 1b). Mutations of residues within the LOV photosensor in the immediate vicinity of the flavin chromophore can strongly increase or decrease the recovery rate constant k_{-1} (Table 1, Figure 1c).[19,20] For example, replacement of a strictly conserved asparagine residue (corresponding to N94 in YF1) in hydrogen-bonding contact with the flavin chromophore by serine, aspartic acid, or alanine resulted in acceleration of dark recovery by between 5- and 45-fold.[21] To the extent they have been tested, mutations modulating the photorecovery kinetics have similar effects between different LOV domains, indicating overarching physical principles. Consequently, alteration by mutagenesis of k_{-1} provides a general and convenient means for modulation of the effective light responsiveness of LOV photoreceptors; if dark recovery is slow (i.e., k_{-1} is small), a comparably low light dose suffices to predominantly populate S_{390} at photostationary equilibrium. However, little is known if and how such photocycle mutations affect the absolute light responsiveness, that is, the rate of the forward reaction $k_1(I)$. Moreover, studies on these mutations have been carried out at the level of isolated LOV photosensor domains, and potential effects on activity and regulation (i.e., K_{dark} and K_{light}) of an associated effector module have generally not been addressed. A recent mutational screen

Table 1. Mutations Accelerating the Photocycle in LOV Photoreceptors

mutation[a]	acceleration photocycle[b]	ref
V28T	21	41
T30A	3.7	36
T30S	3.8	36
N37C	7.5/2	29 and 36
N37V	6.7	36
I39V	5	19
F46H	25	2
R63K	8/13	42 and 36
Q66A	8	38
N94A	45	21
N94D	5	21
N94S	20	21
N104A	2.8	21
N104S	5.6	21
Q123N	87	21

[a]Residue numbers refer to YF1 which derives its LOV domain from *B. subtilis* YtvA. Certain mutations were only studied in the context of other LOV domains. [b]Values as reported by the authors; the effects of mutations were studied at different temperatures.

dx.doi.org/10.1021/sb400205x | *ACS Synth. Biol.* 2014, 3, 811−819

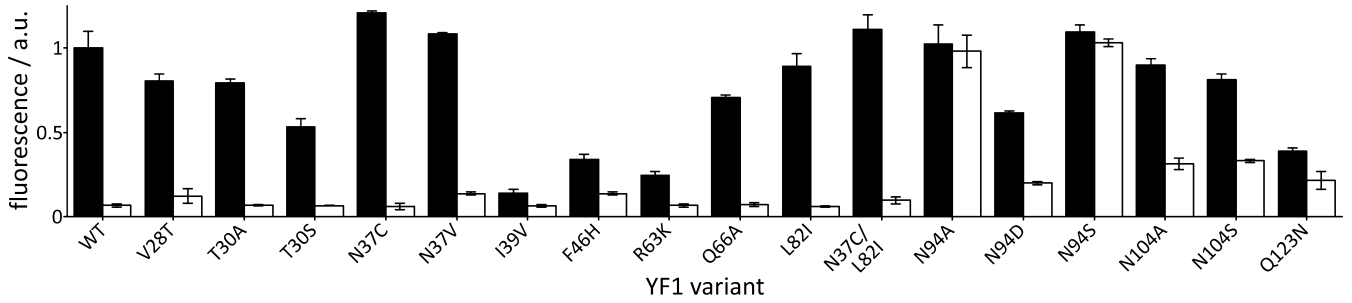

Figure 2. Activity measurements of YF1 variants with the pDusk-DsRed reporter system. For wild-type YF1 blue light (white bars) induces a ~15-fold repression of DsRed reporter fluorescence compared to dark conditions (black bars).

on the engineered LOV photoreceptor YF1[7] revealed that certain mutations that modulate the LOV photocycle kinetics also have adverse effects on regulation, in some cases effectively abolishing the light response.[22]

Here, we report a systematic study on the potential influence of such mutations on light regulation in the blue-light receptor YF1 as a paradigm for LOV proteins. We identify a first group of mutations that lead to impairment of light regulation; mutations from a second group do not have any adverse effects on regulation. Using absorption and electron paramagnetic resonance (EPR) spectroscopy, we investigate the molecular bases for photocycle modulation in mutants from the second group in the proteins YF1 and *As*LOV2.

RESULTS AND DISCUSSION

Effect of Mutations on Photoreceptor Activity. If mutations that modulate LOV photocycle kinetics are to be applied in optogenetics or synthetic biology, it is imperative that they do not impair regulation of a downstream effector module. As pertinent data are missing, we probed these mutations in the context of the engineered photoreceptor YF1[7], which derives its LOV photosensor domain from the *Bacillus subtilis* YtvA protein.[23] In the absence of blue light, YF1 acts as a histidine kinase on the conjugate response regulator FixJ, which upon phosphorylation binds to a cognate promoter and thus activates transcription; in the light, YF1 is converted to a net phosphatase, FixJ is dephosphorylated, FixJ no longer binds to the promoter, and transcriptional activity is down-regulated. We have previously assembled YF1, FixJ, and the cognate promoter on the pDusk-DsRed plasmid to afford light-regulated gene expression in *Escherichia coli*. Expression of the fluorescent reporter DsRed from pDusk is suppressed by around 15-fold under saturating blue light (100 μW cm^{-2}, 470 nm) relative to dark conditions, thus providing a rapid and efficient assay for YF1 activity and regulation[22,24] (Figure 2). We introduced mutations that were previously reported to accelerate the LOV dark recovery (cf. Table 1) into the YF1 protein in the pDusk-DsRed background and measured reporter fluorescence as a function of light. The mutations V28T, T30A, T30S, N37C, N37V, and Q66A had no or at most a modest effect on light regulation and showed behavior similar to wild-type YF1. Notably, residues T30 and N37 are immediately adjacent to each other (cf. Figure 1c), and we reasoned that structural perturbations in this region of the LOV domain might be well tolerated yet accelerate dark recovery kinetics. To test this notion, we focused on the nearby residue leucine 82 and changed it to isoleucine, which occurs at the corresponding position in *As*LOV2 that displays considerably faster dark reversion kinetics; the resultant L82I variant of YF1 showed similar light regulation as wild-type YF1 (Figure 2). By contrast, the variants I39V, F46H, R63K, N94A, N94D, N94S, N104A, and N104S all displayed severely disrupted light regulation, in the case of N94A and N94S effectively lacking any light response (Figure 2). We also found that mutation of the conserved glutamine 123 to asparagine resulted in a YF1 variant that retained a small, yet reproducible light response *in vivo*. This finding is rather unexpected, since photoacoustic measurements on the isolated LOV domain had indicated light-induced structural changes that were much reduced in comparison to wild-type.[21]

Effect of Mutations on Dark Recovery and Absolute Light Responsiveness. Having identified mutations with little or no adverse effect on light regulation in YF1, we set out to characterize certain of these mutations in more detail. For measurements of photocycle kinetics, we expressed and purified wild-type YF1 and the variants N37C, L82I, and N37C/L82I. Using UV/vis absorption spectroscopy, we determined the recovery kinetics for these LOV proteins at 22 °C after saturating illumination with a blue light-emitting diode (LED, 455 nm) (Figure 3a). Time courses could be well described by single-exponential functions or by double-exponential functions with a slower minor phase of less than 20% amplitude. In the latter case, dark recovery rate constants were determined as the rate constant associated with the faster major exponential phase. Dark recovery rate constants k_{-1} amounted to $(1.62 \pm 0.05) \times 10^{-4}$ s^{-1} for YF1 wild-type, $(3.06 \pm 0.13) \times 10^{-4}$ s^{-1} for YF1 L82I, $(6.94 \pm 0.07) \times 10^{-4}$ s^{-1} for YF1 N37C, and $(1.29 \pm 0.10) \times 10^{-3}$ s^{-1} for YF1 N37C/L82I (Table 2). We next assessed the energy barriers associated with dark recovery in the different variants by recording kinetics at different temperatures (Figure 3b). Fitting of the rate constants k_{-1} as a function of temperature yielded Arrhenius activation energies, E_A, of (86.1 ± 8.8) kJ mol^{-1} for YF1 wild-type, (70.3 ± 9.3) kJ mol^{-1} for YF1 L82I, (87.1 ± 9.0) kJ mol^{-1} for YF1 N37C, and (51.7 ± 9.3) kJ mol^{-1} for YF1 N37C/L82I (Table 2, Figure 3c).

To gauge whether the effects of these substitutions are shared across LOV domains, we introduced corresponding mutations into *As*LOV2 as a *de facto* reference protein, which has been widely used in optogenetic and biotechnological applications.[6,25] The structurally equivalent residues of N37 and L82 in YF1 are N425 and I470, respectively, in *As*LOV2. We thus generated the variants N425C, I470L and N425C/I470L of *As*LOV2, where YF1 wild-type corresponds to *As*LOV2 I470L, YF1 L82I corresponds to *As*LOV2 wild-type, YF1 N37C corresponds to *As*LOV2 N425C/I470L, and YF1 N37C/L82I corresponds to *As*LOV2 N425C (cf. Table 2). While the kinetics in the *As*LOV2 variants were much faster than in the

dx.doi.org/10.1021/sb400205x | *ACS Synth. Biol.* 2014, 3, 811−819

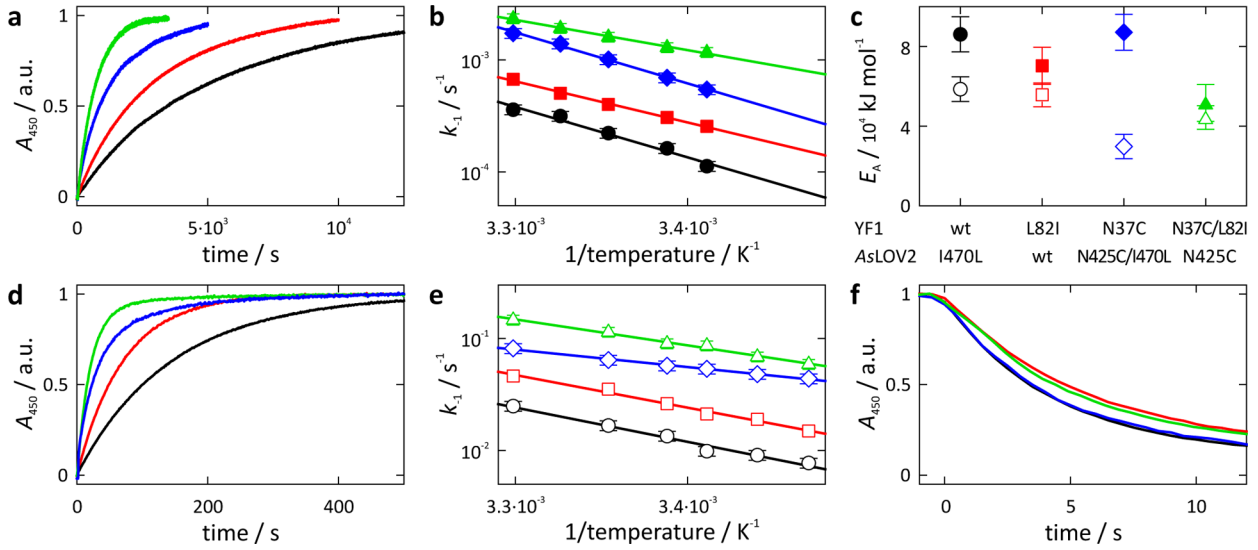

Figure 3. UV/vis absorption spectroscopy on YF1 and *As*LOV2 variants. (a) Photorecovery after excitation with blue light is followed by absorption at 450 nm. YF1 wild-type data are shown in black, YF1 L82I data in red, YF1 N37C data in blue, and YF1 N37C/L82I data in green. (b) Temperature dependence of recovery rate constants for YF1 variants. Colors as in panel a; lines denote fits to determine Arrhenius activation energies. (c) Arrhenius activation energies E_A for temperature dependence of dark recovery rate constants k_{-1} in the YF1 and *As*LOV2 proteins. (d) Photorecovery kinetics of *As*LOV2 I470L (black), *As*LOV2 wild-type (red), *As*LOV2 N425C/I470L (blue), and *As*LOV2 N425C (green). (e) Temperature dependence of recovery rate constants for *As*LOV2 variants. Colors as in panel d. (f) Photoactivation of YF1 variants induced by blue light was monitored by absorption measurements at 450 nm. YF1 wild-type (black) and YF1 N37C (blue) showed similar kinetics; by contrast, photoactivation in YF1 L82I (red) and YF1 N37C/L82I (green) was markedly retarded.

Table 2. Biophysical Parameters for YF1 and *As*LOV2 Variants

YF1[a]					*As*LOV2			
variant	k_{-1} (s^{-1})	E_A ($kJ \cdot mol^{-1}$)	$\Phi_{390}{}^{x}/\Phi_{390}{}^{wt}$	$T_m{}^{C8\alpha}$ (K)	variant	k_{-1} (s^{-1})	E_A ($kJ \cdot mol^{-1}$)	$T_m{}^{C8\alpha}$ (K)
wild-type	$(1.62 \pm 0.05) \cdot 10^{-4}$	86.1 ± 8.8	$\equiv 1$	109.3 ± 2.9	I470L	$(1.34 \pm 0.03) \cdot 10^{-2}$	58.6 ± 6.2	120.6 ± 2.8
L82I	$(3.06 \pm 0.13) \cdot 10^{-4}$	70.3 ± 9.3	0.62 ± 0.02	94.1 ± 2.6	wild-type	$(2.62 \pm 0.08) \cdot 10^{-2}$	55.7 ± 6.0	89.5 ± 3.3
N37C	$(6.94 \pm 0.07) \cdot 10^{-4}$	87.1 ± 9.0	1.01 ± 0.03	72.6 ± 4.3	N425C/I470L	$(5.71 \pm 0.04) \cdot 10^{-2}$	29.8 ± 6.1	80.5 ± 3.6
N37C/L82I	$(1.29 \pm 0.10) \cdot 10^{-3}$	51.7 ± 9.3	0.75 ± 0.02	64.8 ± 3.9	N425C	$(9.00 \pm 0.03) \cdot 10^{-2}$	44.3 ± 6.0	56.7 ± 3.9

[a]Reported values are plus/minus asymptotic standard errors as obtained by Levenberg–Marquardt nonlinear least-squares fitting.

YF1 variants, the different mutations had similar relative effects on dark recovery in both LOV domains (Figure 3d). The slowest recovery kinetics were observed for AsLOV2 I470L ($(1.34 \pm 0.03) \times 10^{-2}$ s^{-1}), followed by *As*LOV2 wild-type ($(2.62 \pm 0.08) \times 10^{-2}$ s^{-1}), *As*LOV2 N425C/I470L ($(5.71 \pm 0.04) \times 10^{-2}$ s^{-1}), and *As*LOV2 N425C ($(9.00 \pm 0.03) \times 10^{-2}$ s^{-1}). The Arrhenius activation energies for dark recovery amounted to (58.6 ± 6.2) kJ mol^{-1} for *As*LOV2 I470L, (55.7 ± 6.0) kJ mol^{-1} for *As*LOV2 wild-type, (29.8 ± 6.1) kJ mol^{-1} for *As*LOV2 N425C/I470L, and (44.3 ± 6.0) kJ mol^{-1} for *As*LOV2 N425C (Figure 3e). The activation energies observed for the different variants displayed a similar trend as those observed in the YF1 variants with the notable exception of *As*LOV2 N425C/I470L, which showed a weak temperature dependence (i.e., E_A is small) while the corresponding YF1 construct N37C showed a strong temperature dependence (i.e., E_A is large).

Considerable effort has been directed at measurements of the dark recovery kinetics (k_{-1}) in LOV domains, arguably because pertinent spectroscopic experiments are straightforward, and resultant effects can be large.[20] As discussed, these mutations provide convenient handles for adjustment of the effective light responsiveness of LOV photoreceptors under photostationary conditions. By contrast, much less attention has been paid to the effect of mutations on the absolute light responsiveness, that is, the overall quantum yield Φ_{390} for formation of the signaling state S_{390} after blue-light absorption, although differences among phototropin photoreceptors had been reported early on.[26−28] To assess whether some of the above mutants affect the absolute light responsiveness, we measured how fast the different YF1 variants assume the signaling state when illuminated with a given blue-light irradiance I (Figure 3f). In the irradiance regime where photoactivation occurs much faster than dark recovery ($k_1(I) \gg k_{-1}$), the observable rate constant, k_{obs}, for the approach to the photostationary state is dominated by the forward kinetics ($k_{obs} \approx k_1(I)$). By comparing to the photoactivation kinetics of YF1 wild-type, we can thus infer relative apparent quantum yields Φ_{390} for the different variants (Table 2). Interestingly, the mutation L82I resulted in an approximately 40% lower apparent quantum yield than wild-type, whereas N37C had little effect; the double mutant N37C/L82I had a 25% reduced apparent quantum yield. For the wild-type of *B. subtilis* YtvA from which the YF1 LOV domain derives, quantum yields Φ_{390} between 0.44 and 0.49 have been reported[11,23] which allows to roughly estimate absolute quantum yields Φ_{390} of about 0.27−0.30 in YF1 L82I and of about 0.33−0.37 in YF1 N37C/L82I.

Effect of Mutations on the Flavin Chromophore Environment. To better understand the molecular bases for the differing dark recovery kinetics and light responsiveness in the YF1 and *As*LOV2 proteins, we employed electron

dx.doi.org/10.1021/sb400205x | *ACS Synth. Biol.* 2014, 3, 811−819

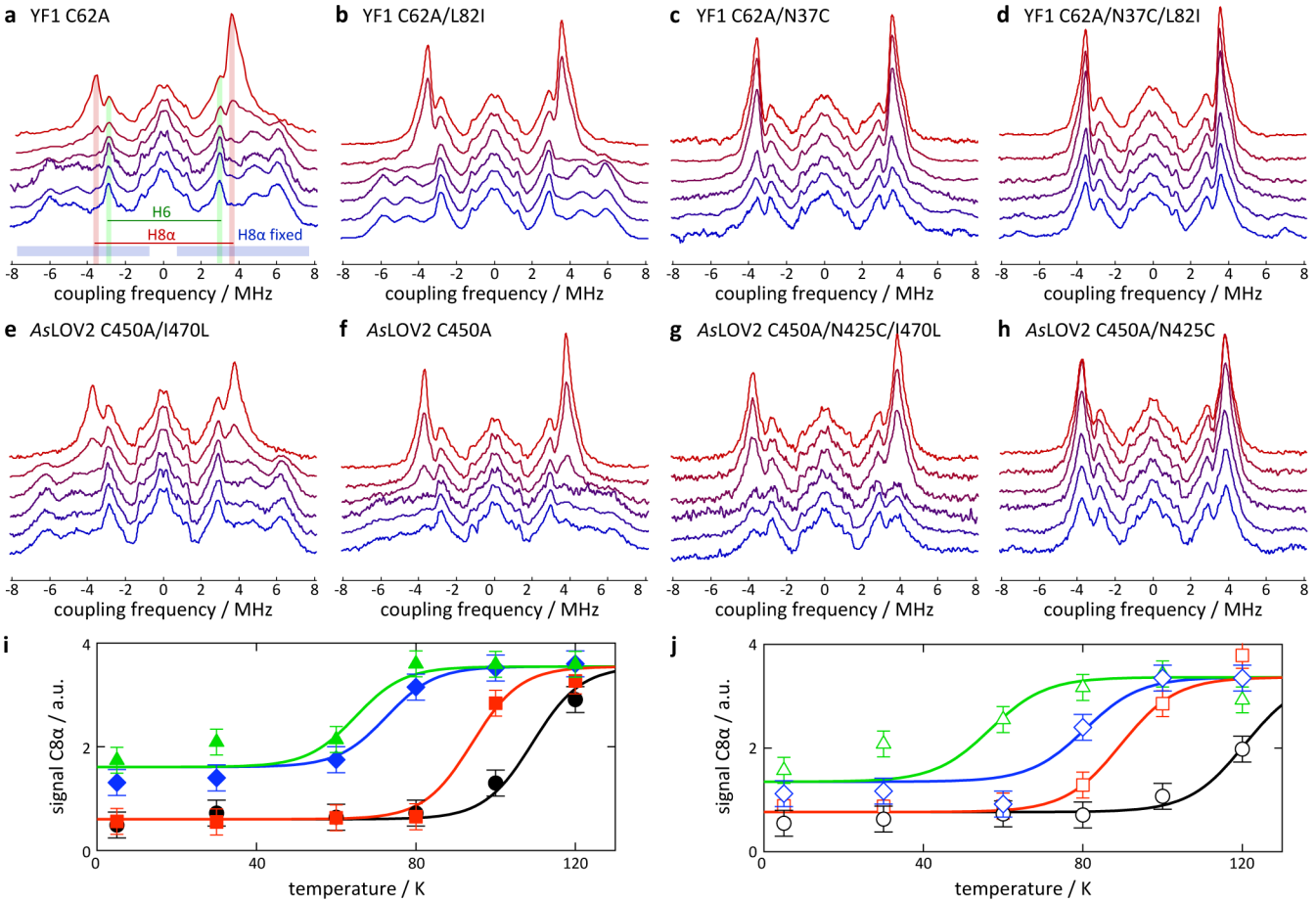

Figure 4. Electron−nuclear double-resonance (ENDOR) measurements on YF1 variants (a−d) and *As*LOV2 variants (e−h). Protein samples were illuminated with 450-nm light and rapidly cryo-cooled in liquid nitrogen. ENDOR spectra were recorded at temperatures of 5, 30, 60, 80, 100, and 120 K (from bottom to top). In all spectra, frequencies are reported relative to the nuclear frequency of free protons. (a) YF1 C62A. Resonance frequencies of the H6 proton, the freely rotating C8α methyl group, and the restricted C8α methyl group are indicated. (b) YF1 C62A/L82I. (c) YF1 C62A/N37C. (d) YF1 C62A/N37C/L82I. (e) *As*LOV2 C450A/I470L. (f) *As*LOV2 C450A. (g) *As*LOV2 C450A/N425C/I470L. (h) *As*LOV2 C450A/N425C. (i) The temperature dependence of the C8α methyl peak amplitudes at around +3.6 MHz in the different YF1 variants (panels a−d) was globally fitted to logistic functions to determine temperature midpoints for the two-state transition between a locked and a freely rotating C8α methyl group (black ○, YF1 C62A; red □, YF1 C62A/L82I; blue ◊, YF1 C62A/N37C; green Δ, YF1 C62A/N37C/L82I). (j) As in panel i but for *As*LOV2 variants (black ○, *As*LOV2 C450A/I470L; red □, *As*LOV2 C450A; blue ◊, *As*LOV2 C450A/N425C/I470L; green Δ, *As*LOV2 C450A/N425C).

paramagnetic resonance (EPR) spectroscopy. Brosi et al. had previously shown by EPR spectroscopy that mutation of an asparagine residue (corresponding to N37 in YF1) to cysteine increases the rotational freedom of the C8α methyl group of the flavin chromophore.[29] Since EPR spectroscopy exclusively reports on paramagnetic molecules (i.e., those with unpaired electron spins), most proteins are inherently insensitive to the method. Unpaired electron spins can be introduced at specific sites (e.g., via labeling with nitroxide compounds)[30] and thus provide a sensitive local probe against very low background signal. In addition to chemical labeling, LOV photoreceptors offer an alternate route for introduction of site-specific spin labels, namely incapacitation by mutagenesis of the conserved, active-site cysteine residue which aborts the standard photocycle. Upon blue-light absorption, the flavin chromophore undergoes efficient intersystem crossing to the triplet state T_{650} which possesses two unpaired electrons (cf. Figure 1a). As reaction to the S_{390} state is blocked in cysteine-deletion variants, the T_{650} state accumulates to significant extent under photostationary conditions, and a local spin probe for the flavin chromophore is provided. The resultant spin density is anisotropically distributed across the isoalloxazine ring with the highest density observed at positions N5, C6, C8α, and C1′. The molecular surroundings of the flavin ring can thus be probed at these positions in electron−nuclear double-resonance (ENDOR) experiments,[29] which detect the hyperfine coupling between electron spins and nearby nuclear spins.

To conduct ENDOR experiments, we replaced the active-site cysteine residue (C62 in YF1 and C450 in *As*LOV2) in the above variants of the two LOV proteins by alanine. Purified samples were illuminated with saturating blue light and immediately cryo-cooled in liquid nitrogen; ENDOR spectra were recorded for frequencies between −8 and +8 MHz relative to the nuclear frequency of free protons (51.7 MHz in the Q-Band) at temperatures of 5, 30, 60, 80, 100, and 120 K (Figure 4). As exemplified for YF1 C62A (Figure 4a), hyperfine couplings can be discerned for the proton at the C6 position (~ ± 3 MHz) and for the methyl group protons at the C8α position. The coupling of the proton at the C1′ position gives rise to a broad band of very low intensity that can, depending on the side chain orientation, partly overlap the C8α methyl group signal. Due to the high spin density on N5 and C4a, the

dx.doi.org/10.1021/sb400205x | *ACS Synth. Biol.* 2014, 3, 811−819

coupling to the proton at the N5 position is very large (around ±15 MHz) and thus falls off the recorded spectral scale. At a temperature of 120 K, the C8α methyl group of YF1 C62A can freely rotate and the three attached protons thus become equivalent (signal at ∼ ± 3.6 MHz). At lower temperatures, rotation of this methyl group around the C8−C8α single bond is increasingly restricted, the C8α methyl protons become nonequivalent, and three distinct coupling peaks are observed in the range of −7.5 to −1 MHz and +1 to +7.5 MHz, respectively. The ENDOR spectra thus report on the local mobility of the C8α methyl group of the chromophore and its surroundings. The YF1 variants C62A/L82I (Figure 4b), C62A/N37C (Figure 4c) and C62A/N37C/L82I (Figure 4d) displayed similar ENDOR spectra but the transition between a freely mobile and a spatially restricted C8α methyl group occurred at successively lower temperatures. In the variants C62A/N37C and C62A/N37C/L82I, even at 5 K a small peak is visible at the frequency of the freely mobile C8α methyl group; this could either reflect residual mobility of the methyl group in the restricted state or it could be due to overlap with the band of one of the three immobile C8α protons.[29] In the *As*LOV2 context, the corresponding mutant variants strikingly showed the same qualitative behavior, with the C450A/I470L variant displaying the transition between mobile and restricted C8α methyl group at the highest temperature and the C450A/N425C variant displaying this transition at the lowest temperature (Figure 4e−h). We used nonlinear least-squares fitting of the signal intensity of the mobile C8α methyl group to estimate midpoint temperatures $T_m^{C8\alpha}$ for the two-state transition between a mobile and a restricted C8α methyl group in the different variants of YF1 (Figure 4i) and *As*LOV2 (Figure 4j). For YF1 C62A a transition temperature of (109.3 ± 2.9) K was obtained whereas the variants C62A/L82I, C62A/N37C and C62A/N37C/L82I yielded successively lower transition temperatures of (94.1 ± 2.6) K, (72.6 ± 4.3) K and (64.8 ± 3.9) K, respectively. In the case of *As*LOV2, the C450A/I470L variant had a $T_m^{C8\alpha}$ of (120.6 ± 2.8) K, the C450A variant had a $T_m^{C8\alpha}$ of (89.5 ± 3.3) K, the C450A/N425C/I470L variant had a $T_m^{C8\alpha}$ of (80.5 ± 3.6) K, and the C450A/N425C variant had a $T_m^{C8\alpha}$ of (56.7 ± 3.9) K.

Correlated Effects on Dark Recovery and Flavin Chromophore Environment. The experimental data on the YF1 variants reveal a striking correlation between the effects of mutations on the dark recovery rates k_{-1} (cf. Figure 3a) and the effects on rotational freedom of the flavin C8α methyl group (cf. Figure 4i). A plot of the natural logarithm of k_{-1} at 22 °C versus the midpoint temperature $T_m^{C8\alpha}$ for the transition between restricted and mobile C8α methyl group yields a linear correlation coefficient of −0.992 with a slope of (−4.51 ± 0.44) × 10^{-2} K^{-1} (Figure 5). Apparently, this correlation is shared between LOV domains as the *As*LOV2 data also display a linear correlation with slightly smaller slope of (−3.22 ± 0.24) × 10^{-2} K^{-1} and a linear correlation coefficient of −0.969.

However, correlation between two quantities should not be considered proof for direct causation. In particular, the effects on the presently measured quantities manifest on quite different temperature scales, namely at ambient temperatures in case of the dark recovery rate constants k_{-1}, and at temperatures between 5 and 120 K in case of the C8α methyl group mobility. We therefore deem it unlikely that the flavin C8α methyl rotation probed by ENDOR spectroscopy directly affects the recovery reaction from the signaling state S_{390} to the dark-adapted ground state D_{447}. Rather, both processes appear

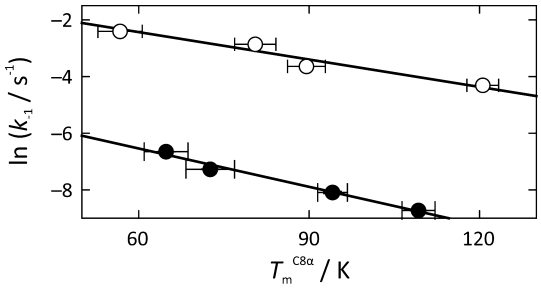

Figure 5. Correlation of biophysical parameters in YF1 and *As*LOV2 variants. The natural logarithm of the dark recovery rate constant k_{-1} at 22 °C is plotted versus the midpoint temperature $T_m^{C8\alpha}$ for the transition between a freely rotating and a restricted C8α methyl group of the flavin chromophore. The linear correlation coefficients for the YF1 variants (●) and the *As*LOV2 variants (○) are −0.948 and −0.969, respectively.

to be affected in similar ways by alterations in the environment of the flavin chromophore. To arrive at a molecular understanding of these effects, we compared the chromophore-binding pockets of YF1 and *As*LOV2 as revealed by high-resolution crystal structures[31,32] (Figure 6). In both proteins

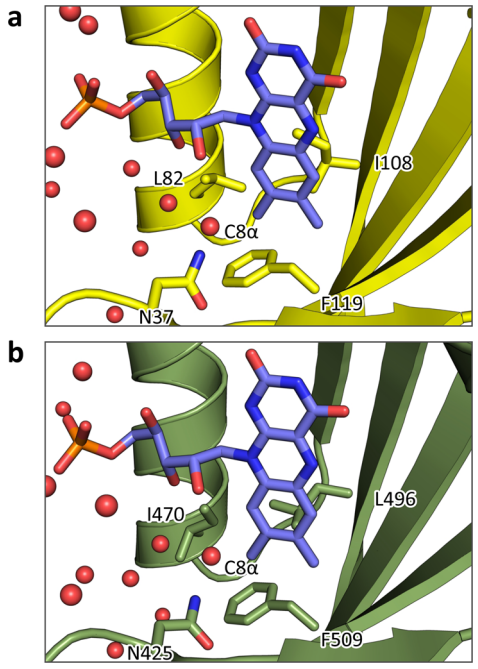

Figure 6. Close-up view of the chromophore-binding pocket in YF1 (panel a, PDB entry 4GCZ[32]) and *As*LOV2 (panel b, 2V0U[31]). In the YF1 structure the terminal Cδ methyl groups of the γ-branched residue leucine 82 bracket the C8α methyl group of the flavin chromophore and thus impair its mobility; by contrast, in *As*LOV2 the β-branched residue isoleucine 470 points away from the flavin ring. Variations of residues N37 in YF1 and N425, L496, and F509 in *As*LOV2 also affect the mobility of the C8α methyl group (cf. Figure 4 and Brosi et al.[29]). Water molecules are shown as red spheres.

the C8α methyl group is tightly embedded between several hydrophobic side chains, deriving from residues T30, N37, L82, I108, and F119 in YF1, and from the corresponding residues T418, N425, I470, L496, and F509 in *As*LOV2. Notably, the side chain of leucine 82 in YF1 is branched at the Cγ atom, which allows the terminal Cδ1 and Cδ2 methyl groups to bracket the C8α methyl group of the flavin chromophore. By

dx.doi.org/10.1021/sb400205x | *ACS Synth. Biol.* 2014, 3, 811−819

contrast, the corresponding residue of *As*LOV2, isoleucine 470, is branched at the Cβ atom which positions its Cγ2 methyl group away from the flavin chromophore. Rotational freedom of the flavin C8α methyl group is evidently governed by the packing of the surrounding hydrophobic residues. As indicated by ENDOR spectroscopy, an isoleucine residue in position 82 of YF1 grants more conformational flexibility than a leucine residue does. Similarly, substitutions of the other above residues in direct contact with the C8α methyl group have been shown to also affect rotational freedom of this methyl group[29] and/or dark recovery kinetics.[33]

These differences in the packing of hydrophobic residues near the flavin ring can also account for the observed difference in dark recovery kinetics. As apparent from the crystal structures of YF1 and *As*LOV2 (cf. Figure 6), a continuous, water-filled crevice extends from the protein surface to the chromophore, and mutations in this region of the LOV photosensor are thus expected to affect solvent access. Dark recovery from the signaling state S_{390} to the ground state D_{447} entails cleavage of the thioether bond between the conserved cysteine residue and atom C4a of the flavin ring (cf. Figure 1a). This process involves initial abstraction of the proton at the flavin position N5 and was shown to be base-catalyzed.[34] Substitutions such as asparagine 37 to cysteine in YF1 might grant more ready solvent access and hence allow water to closely approach the chromophore where it can serve as a general base catalyst. In support of this notion, altered water access to the chromophore has recently been suggested to account for differential photocycle kinetics in *As*LOV2 variants.[35]

Interestingly, the mutation L82I also reduced the absolute light responsiveness (Φ_{390}) of the YF1 photoreceptor (cf. Figure 3f), whereas the mutation N37C had negligible effect. Absolute light responsiveness therefore appears uncorrelated with C8α methyl mobility and dark recovery rates. The molecular basis for the properties of the L82I variant is unclear but may be due to slight changes in the position and orientation of the flavin chromophore thereby making it less conducive to intersystem crossing and subsequent formation of the thioether bond. Our findings are consistent with a recent study which reported that the quantum yield for intersystem crossing in *As*LOV2, that possesses an isoleucine residue in the corresponding position, is only 60% of the value determined for *B. subtilis* YtvA.[11] Effects of mutations on the quantum yield for formation of the LOV signaling state have been reported before (e.g., in Raffelberg et al.)[36] but to date, these mutations have not been exploited in optogenetics and synthetic biology.

Implications for Photoreceptor Applications in Biotechnology and Synthetic Biology. In closing, we note that variations of residues in vicinity of the flavin chromophore provide a convenient avenue for adjusting photocycle kinetics, absolute and effective light responsiveness of LOV photoreceptors as dictated by desired applications in cell biology, biotechnology, and synthetic biology. However, we have shown that mutations can produce unwanted, adverse effects on light regulation (cf. Figure 2)[22] and that they should hence be employed with certain caveats. It remains to be elucidated to what extent the presently tested mutations also impair signaling in other LOV photoreceptors. Tentative evidence that this is indeed the case derives from meticulous mutagenesis studies on *As*LOV2, which revealed that diverse substitutions can strongly affect the extent of light-triggered conformational changes.[33,37] Ideally, the impact of each mutation is tested at the functional level in the context of an intact photoreceptor comprising both photosensor and effector modules. In the absence of such data, we suggest that mutations be focused on residues near the apolar dimethyl-benzene portion of the flavin chromophore which on average are less conserved (e.g., V28, T30, N37, and L82 in YF1). By contrast, replacements of the highly conserved polar amide residues that form hydrogen bonds to the flavin chromophore (e.g., N94, N104 and Q123 in YF1) impair light regulation, with just a few exceptions (e.g., the mutation Q66A).[38] More broadly, the above considerations may not just apply to LOV proteins but to other photoreceptors as well, such as to the red-light sensitive phytochromes, which are widely used in synthetic biology.[39]

METHODS

Molecular Biology and Protein Expression. The gene encoding the *Avena sativa* phototropin 1 LOV2 domain (*As*LOV2, residues 404−546) was amplified by PCR from an earlier expression construct[31] and cloned into the pET-28c vector (Novagen) using *NdeI*/*Sal*I to yield plasmid pET-28c-*As*LOV2. Mutants of *As*LOV2 and YF1 were generated by site-directed mutagenesis in the background of the pET-28c-*As*LOV2 and pET-41a-YF1[32] plasmids, respectively, according to the QuickChange protocol (Invitrogen, Life Technologies GmbH). For assaying YF1 activity *in vivo*, corresponding mutations were also introduced into the pDusk-myc-DsRed vector.[32] All constructs were confirmed by DNA sequencing (GATC Biotech, Konstanz, Germany).

For purification of *As*LOV2, *Escherichia coli* CmpX13 cells[40] were transformed with pET-28c-*As*LOV2 and were used to inoculate twice 1 L LB medium containing 50 μg mL^{-1} kanamycin (denoted LB/Kan in the following), supplemented with 50 μM riboflavin. The culture medium was incubated at 37 °C and 225 rpm until optical density at 600 nm (OD_{600}) reached ∼0.6, at which point temperature was lowered to 16 °C and protein expression was induced by addition of 1 mM β-D-1-thiogalactopyranoside. Following incubation at 16 °C and 225 rpm for ∼18 h, cells were spun down and suspended in buffer A (50 mM Tris/HCl pH 8.0, 20 mM NaCl, 20 mM imidazole, protease inhibitor cocktail Complete Ultra [Roche Diagnostics]). Following lysis by sonication, the supernatant was cleared by centrifugation and applied to a 5-mL Ni^{2+} affinity column (HisPur Ni-NTA Resin, Thermo Scientific) using an Äkta prime plus chromatography system (GE Healthcare). Protein was eluted with a gradient from 0 to 1000 mM imidazole. Based on analysis by gel electrophoresis, elution fractions were pooled and dialyzed into storage buffer (10 mM Tris/HCl pH 8.0, 10 mM NaCl, 10% (v/v) glycerol). Solutions were concentrated using a 10 000-Da cutoff filtration device, and protein concentration was determined by absorption measurements (8453 UV−vis spectrophotometer, Agilent Technologies) using an extinction coefficient at 450 nm of 12,500 M^{-1} cm^{-1}. Site-directed mutants of *As*LOV2 were expressed and purified accordingly. Expression and purification of YF1 and its variants were carried out as described.[32]

YF1 *In Vivo* Activity Assays. The effect of site-directed mutations in YF1 on light regulation was assessed *in vivo* as described.[24,32] Briefly, 5-mL LB/Kan cultures were inoculated with *E. coli* CmpX13 clones harboring the pDusk-myc-DsRed plasmid encoding wild-type YF1 or plasmid variants encoding site-directed mutants of YF1; for each clone, three separate cultures were incubated overnight at 37 °C and 225 rpm in the dark or under constant blue light (470 nm, 100 μW cm^{-2}).

Following incubation and appropriate dilution in 10 mM Tris/HCl pH 8.0, 10 mM NaCl, OD_{600} and DsRed fluorescence were measured in these cultures using black-walled 96-well μClear plates (Greiner BioOne, Frickenhausen, Germany) in a Tecan Infinite M200 PRO plate reader (Tecan Group Ltd. Männedorf, Switzerland). Fluorescence excitation and emission wavelengths were set at 554 ± 9 nm and 591 ± 20 nm, respectively. Data were normalized to the fluorescence per OD_{600} for YF1 under dark conditions and represent the averages of three biological replicates ± standard deviation.

Absorption Spectroscopy. UV/vis absorption measurements were conducted with an Agilent 8453 diode-array spectrophotometer. For the measurement of dark-recovery kinetics, solutions of YF1, *As*LOV2 and variants were exposed to 455-nm light (84 mW cm^{-2}) until the photostationary state was reached. Samples were then kept in the dark, and recovery kinetics were followed by recording absorption spectra. To prevent inadvertent LOV photoactivation by the probe light, the UV lamp of the instrument was turned off; measurements conducted at different sampling rates revealed that under these conditions the probe light does not lead to significant LOV photoactivation. Rate constants for photorecovery k_{-1} were determined by fitting to exponential functions.

For the determination of Arrhenius activation energies, protein samples were equilibrated at temperatures between 15 and 30 °C with a Peltier element, and recovery kinetics after saturating blue-light illumination were recorded. Rate constants as a function of temperature were fitted to the Arrhenius equation $k_{-1}(T) = A \cdot \exp(-E_A/RT)$.

To estimate absolute light sensitivities in YF1 variants, we lowered the blue-light irradiance to 10 mW cm^{-2} and illuminated the samples at 22 °C. Rate constants k_{obs} for the approach to the photostationary state were determined by fitting to exponential functions. Under these conditions, k_{obs} is between 0.15 and 0.25 s^{-1} for the different YF1 variants; since this is much faster than dark recovery (k_{-1}), the observable kinetics are dominated by the forward reaction, and $k_{obs} \approx k_1$. Relative quantum yields for the formation of the S_{390} state Φ_{390} were determined by referencing to wild-type YF1 according to $\Phi^{x}_{390}/\Phi^{wt}_{390} = k^{x}_{obs}/k^{wt}_{obs}$.

Data evaluation was carried out with Origin (OriginLab, Northampton, MA, U.S.A.) and proFit (QuantumSoft, Uetikon am See, Switzerland).

Electron-Paramagnetic Resonance Spectroscopy. For EPR spectroscopy, the YF1 and *As*LOV2 samples were transferred into quartz tubes (QSIL GmbH, Ilmenau, Germany; inner and outer diameters of 1.2 mm and 1.6 mm, respectively), illuminated with a 450-nm LED (LUXEON Lumiled, Phillips Lumileds, San Jose, CA, U.S.A.), and rapidly frozen in liquid nitrogen. Q-band pulsed ENDOR spectra were recorded using a commercial pulse EPR spectrometer Bruker E580 (Bruker BioSpin GmbH, Rheinstetten, Germany) in conjunction with a cavity ENDOR resonator Bruker EN5107D2. For radio frequency pulse generation a Bruker DICE2 frequency generator in conjunction with an Amplifier Research Model 250A250A 250W RF amplifier (Amplifier Research, Souderton, PA, U.S.A.) were used. Cryogenic temperatures were set with an Oxford CF-935 cryostat (Oxford Instruments, Oxfordshire, U.K.) and were controlled using an Oxford ITC503 temperature controller. For Davies-type ENDOR, a microwave pulse sequence $\pi - t - \pi/2 - \tau - \pi$ using 40 and 80 ns $\pi/2$ and π pulses, respectively, and a radio frequency pulse of 15 μs duration starting 1 μs after the first microwave pulse were used. The separation times t and τ between the microwave pulses were set to 18 μs and 300 ns, respectively. The repetition time for the entire pulse pattern was adapted for each temperature so as to exclude any saturation effect due to the long T_1 relaxation time of the flavin radical. The repetition time thus varied from 10 ms at 120 K to 2 s at 5 K. Notably, 2 s is the longest repetition time the instrument supports, and consequently to some degree saturation could not be avoided at 5 K. All ENDOR spectra were recorded at magnetic-field values corresponding to the maximum intensity of the EPR spectrum of the flavin radical. To determine temperature midpoints $T_m^{C8\alpha}$ for the two-state transition between a freely rotating and a restricted C8α methyl group, the peak amplitude for the C8α methyl signal (at ∼ +3.6 MHz) was determined for the individual EPR spectra. The temperature dependence of the magnitude of the C8α methyl signal was globally fitted to phenomenological logistic functions $f(T) = A + C/(1 + \exp(-B(T - T_m^{C8\alpha})))$ using proFit.

AUTHOR INFORMATION

Corresponding Authors

*Tel. +49-30-2093-8850. Fax +49-30-2093-8948. E-mail andreas.moeglich@hu-berlin.de.

*Tel. +49-30-838-56049. Fax +49-30-838-56046. E-mail robert.bittl@fu-berlin.de.

Present Address

[‖](T.G.) Universität Freiburg, Institut für Mikrosystemtechnik (IMTEK), Lehrstuhl für Anwendungsentwicklung, Freiburg, Germany

Author Contributions

[§]R.P.D. and C.E. contributed equally.

Notes

The authors declare no competing financial interest.

ACKNOWLEDGMENTS

We thank members of the Bittl and Möglich groups for discussion. Funding through a Sofja–Kovalevskaya Award by the Alexander-von-Humboldt Foundation (A.M.), by Deutsche Forschungsgemeinschaft within FOR1279 (A.M.) and within the Cluster of Excellence in Catalysis 'UniCat' (R.B.) is gratefully acknowledged.

ABBREVIATIONS

*As*LOV2, *Avena sativa* phototropin 1 LOV2 domain; ENDOR, electron–nuclear double-resonance; EPR, electron paramagnetic resonance; LED, light-emitting diode; LOV, light-oxygen-voltage

REFERENCES

(1) Hegemann, P. (2008) Algal sensory photoreceptors. *Annu. Rev. Plant Biol. 59*, 167–189.

(2) Möglich, A., and Moffat, K. (2010) Engineered photoreceptors as novel optogenetic tools. *Photochem. Photobiol. Sci. 9*, 1286–1300.

(3) Deisseroth, K., Feng, G., Majewska, A. K., Miesenböck, G., Ting, A., and Schnitzer, M. J. (2006) Next-generation optical technologies for illuminating genetically targeted brain circuits. *J. Neurosci. 26*, 10380–10386.

(4) Nagel, G., Ollig, D., Fuhrmann, M., Kateriya, S., Musti, A. M., Bamberg, E., and Hegemann, P. (2002) Channelrhodopsin-1: A light-gated proton channel in green algae. *Science 296*, 2395–2398.

(5) Zhang, F., Wang, L.-P., Brauner, M., Liewald, J. F., Kay, K., Watzke, N., Wood, P. G., Bamberg, E., Nagel, G., Gottschalk, A., and Deisseroth, K. (2007) Multimodal fast optical interrogation of neural circuitry. *Nature 446*, 633–639.

(6) Wu, Y. I., Frey, D., Lungu, O. I., Jaehrig, A., Schlichting, I., Kuhlman, B., and Hahn, K. M. (2009) A genetically encoded photoactivatable Rac controls the motility of living cells. *Nature 461*, 104−108.
(7) Möglich, A., Ayers, R. A., and Moffat, K. (2009) Design and signaling mechanism of light-regulated histidine kinases. *J. Mol. Biol. 385*, 1433−1444.
(8) Christie, J. M., Reymond, P., Powell, G. K., Bernasconi, P., Raibekas, A. A., Liscum, E., and Briggs, W. R. (1998) Arabidopsis NPH1: A flavoprotein with the properties of a photoreceptor for phototropism. *Science 282*, 1698−1701.
(9) Herrou, J., and Crosson, S. (2011) Function, structure and mechanism of bacterial photosensory LOV proteins. *Nat. Rev. Microbiol. 9*, 713−723.
(10) Kottke, T., Heberle, J., Hehn, D., Dick, B., and Hegemann, P. (2003) Phot-LOV1: Photocycle of a blue-light receptor domain from the green alga *Chlamydomonas reinhardtii*. *Biophys. J. 84*, 1192−1201.
(11) Song, S.-H., Madsen, D., van der Steen, J. B., Pullman, R., Freer, L. H., Hellingwerf, K. J., and Larsen, D. S. (2013) Primary photochemistry of the dark- and light-adapted states of the YtvA protein from *Bacillus subtilis*. *Biochemistry 52*, 7951−7963.
(12) Salomon, M., Eisenreich, W., Dürr, H., Schleicher, E., Knieb, E., Massey, V., Rüdiger, W., Muller, F., Bacher, A., and Richter, G. (2001) An optomechanical transducer in the blue light receptor phototropin from *Avena sativa*. *Proc. Natl. Acad. Sci. U.S.A. 98*, 12357−12361.
(13) Harper, S. M., Neil, L. C., and Gardner, K. H. (2003) Structural basis of a phototropin light switch. *Science 301*, 1541−1544.
(14) Yao, X., Rosen, M. K., and Gardner, K. H. (2008) Estimation of the available free energy in a LOV2-J α photoswitch. *Nat. Chem. Biol. 4*, 491−497.
(15) Strickland, D., Yao, X., Gawlak, G., Rosen, M. K., Gardner, K. H., and Sosnick, T. R. (2010) Rationally improving LOV domain-based photoswitches. *Nat. Methods 7*, 623−626.
(16) Volkman, B. F., Lipson, D., Wemmer, D. E., and Kern, D. (2001) Two-state allosteric behavior in a single-domain signaling protein. *Science 291*, 2429−2433.
(17) Jacob, F., and Monod, J. (1961) Genetic regulatory mechanisms in the synthesis of proteins. *J. Mol. Biol. 3*, 318−356.
(18) Möglich, A., Ayers, R. A., and Moffat, K. (2009) Structure and signaling mechanism of Per-ARNT-Sim domains. *Structure 17*, 1282−1294.
(19) Christie, J. M., Corchnoy, S. B., Swartz, T. E., Hokenson, M., Han, I. S., Briggs, W. R., and Bogomolni, R. A. (2007) Steric interactions stabilize the signaling state of the LOV2 domain of phototropin 1. *Biochemistry 46*, 9310−9319.
(20) Zoltowski, B. D., Vaccaro, B., and Crane, B. R. (2009) Mechanism-based tuning of a LOV domain photoreceptor. *Nat. Chem. Biol. 5*, 827−834.
(21) Raffelberg, S., Mansurova, M., Gärtner, W., and Losi, A. (2011) Modulation of the photocycle of a LOV domain photoreceptor by the hydrogen-bonding network. *J. Am. Chem. Soc. 133*, 5346−5356.
(22) Gleichmann, T., Diensthuber, R. P., and Möglich, A. (2013) Charting the signal trajectory in a light-oxygen-voltage photoreceptor by random mutagenesis and covariance analysis. *J. Biol. Chem. 288*, 29345−29355.
(23) Losi, A., Polverini, E., Quest, B., and Gärtner, W. (2002) First evidence for phototropin-related blue-light receptors in prokaryotes. *Biophys. J. 82*, 2627−2634.
(24) Ohlendorf, R., Vidavski, R. R., Eldar, A., Moffat, K., and Möglich, A. (2012) From dusk till dawn: One-plasmid systems for light-regulated gene expression. *J. Mol. Biol. 416*, 534−542.
(25) Strickland, D., Moffat, K., and Sosnick, T. R. (2008) Light-activated DNA binding in a designed allosteric protein. *Proc. Natl. Acad. Sci. U.S.A. 105*, 10709−10714.
(26) Sakai, T., Kagawa, T., Kasahara, M., Swartz, T. E., Christie, J. M., Briggs, W. R., Wada, M., and Okada, K. (2001) Arabidopsis nph1 and npl1: Blue light receptors that mediate both phototropism and chloroplast relocation. *Proc. Natl. Acad. Sci. U.S.A. 98*, 6969−6974.
(27) Christie, J. M. (2007) Phototropin blue-light receptors. *Annu. Rev. Plant Biol. 58*, 21−45.
(28) Kaiserli, E., Sullivan, S., Jones, M. A., Feeney, K. A., and Christie, J. M. (2009) Domain swapping to assess the mechanistic basis of Arabidopsis phototropin 1 receptor kinase activation and endocytosis by blue light. *Plant Cell 21*, 3226−3244.
(29) Brosi, R., Illarionov, B., Mathes, T., Fischer, M., Joshi, M., Bacher, A., Hegemann, P., Bittl, R., Weber, S., and Schleicher, E. (2010) Hindered rotation of a cofactor methyl group as a probe for protein-cofactor interaction. *J. Am. Chem. Soc. 132*, 8935−8944.
(30) Engelhard, C., Raffelberg, S., Tang, Y., Diensthuber, R. P., Möglich, A., Losi, A., Gärtner, W., and Bittl, R. (2013) A structural model for the full-length blue light-sensing protein YtvA from *Bacillus subtilis*, based on EPR spectroscopy. *Photochem. Photobiol. Sci. 12*, 1855−1863.
(31) Halavaty, A. S., and Moffat, K. (2007) N- and C-terminal flanking regions modulate light-induced signal transduction in the LOV2 domain of the blue light sensor phototropin 1 from *Avena sativa*. *Biochemistry 46*, 14001−14009.
(32) Diensthuber, R. P., Bommer, M., Gleichmann, T., and Möglich, A. (2013) Full-length structure of a sensor histidine kinase pinpoints coaxial coiled coils as signal transducers and modulators. *Structure 21*, 1127−1136.
(33) Zayner, J. P., Antoniou, C., and Sosnick, T. R. (2012) The amino-terminal helix modulates light-activated conformational changes in AsLOV2. *J. Mol. Biol. 419*, 61−74.
(34) Alexandre, M. T., Arents, J. C., van Grondelle, R., Hellingwerf, K. J., and Kennis, J. T. (2007) A base-catalyzed mechanism for dark state recovery in the *Avena sativa* phototropin-1 LOV2 domain. *Biochemistry 46*, 3129−3137.
(35) Zayner, J. P., and Sosnick, T. R. (2014) Factors that control the chemistry of the LOV domain photocycle. *PLoS One 9*, e87074.
(36) Raffelberg, S., Gutt, A., Gärtner, W., Mandalari, C., Abbruzzetti, S., Viappiani, C., and Losi, A. (2013) The amino acids surrounding the flavin 7a-methyl group determine the UVA spectral features of a LOV protein. *Biol. Chem. 394*, 1517−1528.
(37) Zayner, J. P., Antoniou, C., French, A. R., Hause, R. J., Jr., and Sosnick, T. R. (2013) Investigating models of protein function and allostery with a widespread mutational analysis of a light-activated protein. *Biophys. J. 105*, 1027−1036.
(38) Zoltowski, B. D., Nash, A. I., and Gardner, K. H. (2011) Variations in protein-flavin hydrogen bonding in a light, oxygen, voltage domain produce non-Arrhenius kinetics of adduct decay. *Biochemistry 50*, 8771−8779.
(39) Shimizu-Sato, S., Huq, E., Tepperman, J. M., and Quail, P. H. (2002) A light-switchable gene promoter system. *Nat. Biotechnol. 20*, 1041−1044.
(40) Mathes, T., Vogl, C., Stolz, J., and Hegemann, P. (2009) *In vivo* generation of flavoproteins with modified cofactors. *J. Mol. Biol. 385*, 1511−1518.
(41) Kawano, F., Aono, Y., Suzuki, H., and Sato, M. (2013) Fluorescence Imaging-based high-throughput screening of fast- and slow-cycling LOV proteins. *PLoS One 8*, e82693.
(42) Tang, Y., Cao, Z., Livoti, E., Krauss, U., Jaeger, K.-E., Gärtner, W., and Losi, A. (2010) Interdomain signalling in the blue-light sensing and GTP-binding protein YtvA: A mutagenesis study uncovering the importance of specific protein sites. *Photochem. Photobiol. Sci. 9*, 47−56.